

NIST-GCR-98-746

**Critical Mass Pyrolysis Rates for Extinction in Fires
Over Solid Materials**

Michael A. Delichatsios
Factory Mutual Research Corporation
Norwood, MA 02062

NIST

**United States Department of Commerce
Technology Administration
National Institute of Standards and Technology**

NIST-GCR-98-746

Critical Mass Pyrolysis Rates for Extinction in Fires Over Solid Materials

Prepared for
U.S. Department of Commerce
National Institute of Standards and Technology
Gaithersburg, MD 20899

By
Michael A. Delichatsios
Factory Mutual Research Corporation
Norwood, MA 02062

December 1996
Issued April 1998



ABSTRACT

New flame extinction conditions for the critical mass pyrolysis rate are developed when extinction occurs by interaction of flames with the pyrolyzing surface of a condensed material. The extinction conditions provide the critical mass pyrolysis rate and the corresponding convective heat flux to the surface. A novel chemistry based formulation for extinction is provided which shows that the sum of fuel mass fraction near the surface and the ambient oxygen mass fraction (corrected for stoichiometry and combustion efficiency) is constant. The extinction conditions are derived from simple analysis of combustion and heat transfer, and they are shown to be applicable for various experimental conditions such as fuel dilution by inert gas, oxygen dilution by inert gas, effects of external heat flux, material preheating, transient (charring) pyrolysis, including geometric effects which influence the critical mass pyrolysis rate through an effective heat transfer coefficient. Additional validation of the proposed extinction conditions is provided by numerical simulation reported in literature in the regime of low straining rates for a stagnation flow on a cylinder. The present approach can be used to measure critical extinction conditions in a flammability apparatus and allow them to be applied in other conditions such as in microgravity. The critical extinction conditions are needed to calculate transient decay pyrolysis of solids after an extinguishment agent is applied.

Notice

This report was prepared for the Building and Fire Research Laboratory of the National Institute of Standards and Technology under grant number GONANB4D1675. The statement and conclusions contained in this report are those of the authors and do not necessarily reflect the views of the National Institute of Standards and Technology or the Building and Fire Research Laboratory.

TABLE OF CONTENTS

<u>Section</u>	<u>Title</u>	<u>Page</u>
ABSTRACT		i
ACKNOWLEDGMENTS		ii
I	INTRODUCTION	1
II	ENERGY BALANCE AT SOLID FUEL SURFACE	3
	2.1 Flame Convective Heat Fluxes	6
	2.2 Fuel Dilution by an Inert Gas	13
	2.3 Oxidant Stream Depletion by Nitrogen	16
III	CRITICAL PYROLYSIS RATES FOR VARYING SURFACE WATER DROP APPLICATION RATES	23
IV	CRITICAL PYROLYSIS RATES AT EXTINCTION FOR CHARRING MATERIALS	27
V	DISCUSSION	31
VI	CONCLUSIONS	34
REFERENCES		35

LIST OF FIGURES

<u>Figure</u>	<u>Title</u>	<u>Page</u>
1	Expected convective heat flux variation with total mass pyrolysis rate and definition of steady pyrolysis state (point A) and critical conditions for extinction (point A*).	5
2a	Heat transfer data to the porous burner: Ethane-nitrogen system (porous burner diameter 4 in., lip height 1/4 in.). Solid symbols represent convective heat fluxes, open symbols total heat fluxes; λ is the air to fuel mole stoichiometric ratio, U is the average fuel gas velocity at the burner (from ref. 9).	9
2b	Convective heat flux to the porous burner versus the mass flux multiplied by the air to fuel mass stoichiometric ratio (data are taken from Figure 2a). The abscissa is proportional to the ethane mass flux rate.	10
2c	Effects of diameter on critical fuel mass flux and total heat transfer flux to the burner for propane; U is the average fuel gas velocity at the burner (from ref. 9).	15
3a	Mass pyrolysis rate of PMMA as a function of external heat flux at constant values of various oxygen mole fractions, .21, .19, .18, .17, .14, .13, .12, .115 (from Tewarson ¹⁰).	17
3b	Variations of external heat flux and mole fraction of oxygen for constant mass burning rates, $\dot{m}'' = 12, 10, 7, 5$ (extinction limit) g/m^2s . Same data as in Figure 3a (from Tewarson ¹⁰).	18
3c	The effect of initial sample temperature T_0 on normalized critical oxygen concentration $OI(T_0)/OI(298\text{ K})$ and on linear regression rate U for a sample 1 cm in diameter : 1-PS; 2-PMMA; 3-POM (from ref. 11).	19
3d	Total heat flux at critical pyrolysis rate for PMMA results shown in Figures 3a and 3c.	20
4	Burning rate of vertical PMMA slabs versus external radiant flux for various water application rates (ref. 12).	24
5	Factory Mutual Flammability Apparatus where both external heat flux and oxidant concentrations can be varied (ref. 17) for measuring extinction on solid fires.	28

LIST OF FIGURES

<u>Figure</u>	<u>Title</u>	<u>Page</u>
6a	Mass loss rate for particle board until flame extinction occurs at 400 s for the following conditions: external heat flux 35 kW/m ² , at ambient air. Flame extinction is observed visually and supported by measurements as shown in Fig. 6b and 6c.	29
6b	Oxygen consumption for the test described in Fig. 6a: extinction is indicated to occur at 400 s.	30
6c	Carbon monoxide production for test described in Fig. 6a: extinction is indicated to occur at about 400 s, where a sudden increase of CO production occurs.	30
7	Computed and experimental mass flux at extinction conditions normalized by the heat transfer coefficient in terms of straining rate, α , in counterflow diffusion flame on a cylinder. At low straining rates, extinction mass flux is nearly constant (independent of straining rate) in accordance with present results (Eq. 9).	32

LIST OF TABLES

<u>Table</u>	<u>Title</u>	<u>Page</u>
I	Combustion Efficiency at Critical Mass Flux Rates for Ethane-Nitrogen Gas Burners	13
II	Heat Fluxes for PMMA (Fig. 3a)	22
III	Estimated Convective Heat Flux at Extinction in Water Application Tests - Dilution Effects (See Fig. 4)	26

I

INTRODUCTION

We present a definitive way for determining extinction conditions of a fire over a pyrolyzing surface when the mass pyrolysis rate decreases owing to the action of an extinguishment agent (such as water on the surface or a gaseous agent) or owing to transient pyrolysis resulting from char formation. The simple methodology, described in this work, also leads to practical measurements of extinction conditions for a fire over any given material by using small scale flammability apparatus.

The proposed model attempts to bridge the gap between analytical (including numerical) investigations and empirical criteria for critical mass pyrolysis rates at extinction. Analytical solutions are based on asymptotic methods of combustion for a single Arrhenius reaction founded on methodologies developed by Russian scientists⁽¹⁾, Friedlander⁽²⁾, Fendell⁽³⁾, and Linan⁽⁴⁾. In these models, the gaseous reactions are modified by interaction with the surface pyrolysis rates through an energy balance (Law⁽⁵⁾, Sibulkin⁽⁶⁾). These analytical models and results have the following drawbacks:

1. They do not separate clearly the gaseous combustion dynamics from the energy balance near the surface, so that the physics of extinction can be clearly visualized.
2. As a consequence, it is not transparent how to use these (asymptotic) analytical results to characterize extinction of fires over a solid material, considering the fact that: a) analytical solutions use assumed (1-step, usually) kinetics; and b) the chemical kinetics of a solid material are not known.

On the practical side, several empirical conditions have been proposed for critical pyrolysis extinction conditions (see Beyler⁽⁷⁾ for a systematic discussion). The empirical conditions can be classified as:

- 1) Near extinction, the flame temperature decreases below a critical value owing to cooling by the surface^(7,8);
 - 2) Near extinction, the mass pyrolysis rate is less than some critical mass pyrolysis rate^(7,8);
- and
- 3) Near extinction, the flame heat flux to the surface is proportional to mass pyrolysis rate⁽⁸⁾.

Each of these empirical conditions contain only part of the true extinction conditions, but they are all inconsistent and deficient in certain applications⁽⁷⁾; their deficiencies are not further elaborated in this report.

The new extinction conditions presented in this work are derived first in the following two sections by separating the dynamics of gaseous reaction from the energy balance in the solid material using a simple physical interpretation; validation by comparison with experiments is established next followed by discussion, comparison with analytical solutions and conclusions.

II

ENERGY BALANCE AT SOLID FUEL SURFACE

For steady state flames over a solid fuel, an energy balance equation at the surface relates mass pyrolysis rates to imposed heat fluxes and heat drains such as by water application:

$$\dot{m}_p'' \Delta h_v + \dot{m}_w'' L_w = \dot{q}_c'' - \dot{q}_{rr}'' + \dot{q}_{rf}'' + \dot{q}_e'' \quad (1)$$

Here, \dot{m}_p'' is the mass pyrolysis rate, ΔH is the effective heat of pyrolysis, \dot{m}_w'' is the water application rate, L_w is the effective heat for water vaporization; in addition, \dot{q}_c'' , \dot{q}_{rr}'' , \dot{q}_{rf}'' , \dot{q}_e'' are convective, reradiative, flame radiation, and external heat fluxes, respectively.

Near extinction, as the mass pyrolysis rate decreases (for example, due to water application or oxidant inerting), steady (gaseous) flames can no longer exist. This causes the pyrolysis rate to further decay and eventually decrease to zero if no external heat flux is imposed. The critical pyrolysis rate at extinction is defined as the minimum pyrolysis rate for which steady burning exists, namely, when both the energy balance Eq. (1) is applicable and a steady gaseous flame is established over the solid fuel. It would also be interesting (but outside of the scope of this work) to compare extinction of ongoing burning solid to the piloted ignition of the same solid being heated until pyrolysis occurs.

We can simplify the extinction problem in an effective way for understanding the physics by observing that a crucial connection is manifested between the energy balance, Eq. (1), and gaseous combustion dynamics through the convective term \dot{q}_c'' . We proceed by writing Eq. (1) as:

$$\dot{m}_p'' \left(\Delta H_v + \frac{\dot{m}_w'' L_w}{\dot{m}_p''} + \frac{\dot{q}_{rr}''}{\dot{m}_p''} - \frac{\dot{q}_{rf}''}{\dot{m}_p''} - \frac{\dot{q}_e''}{\dot{m}_p''} \right) = \dot{q}_c'' \quad (2a)$$

or equivalently,

$$\dot{m}_p'' \Delta H_v = \dot{q}_c'' \quad (2b)$$

where ΔH_v is equal to the term inside the parenthesis of Eq. (2a). For steady state conditions, Eq. (2a) may be considered equivalent to Eq. (2b), where ΔH_v is considered to have a fixed value.

For the present steady state pyrolysis conditions, we also consider that the solid fuel surface temperature is fixed (for example, equal to a "pyrolysis" temperature).

We can now decouple the gas combustion dynamics from the surface energy balance (Eqs. (2a) and (2b)) by considering the following burning problem: given a surface fuel pyrolysis rate \dot{m}_p'' at a fixed surface temperature T_w , how does the convective heat flux, \dot{q}_c'' , from an established diffusion flame (fire) near the surface vary as \dot{m}_p'' decreases until flame extinction occurs? The flow field near the surface can be generated by buoyancy, or by a fixed flow, or be controlled by diffusional transport only. The present approach and analysis is valid and applicable even though the radiant heat flux (\dot{q}_{rr}'' in Eq. 2a) varies with the mass pyrolysis rate because: a) we consider steady state conditions, and b) the radiant heat flux decreases monotonically with pyrolysis (mass blowing) rate⁽⁹⁾.

Figure 1 illustrates the present concept. In this figure the convective heat flux is plotted as function of mass pyrolysis rate for a gaseous porous pool burner. As mass pyrolysis rate decreases, the convective heat flux increases because surface blowing is reduced until a maximum value of the convective heat flux is reached (Branch I in Fig. 1). Further decrease in pyrolysis rate is followed by decrease in the convective heat flux because the flame approaches the surface and partial flame quenching occurs leading eventually to complete extinction of flames (Branch II in Figure 1). More details shown in Fig. 1 are discussed in the next section.

The mass flux corresponding to the maximum convective heat flux may be identified as the critical mass flux for extinction of a condensed material fire, as can be seen by examining the conditions for stable steady state burning of a condensed material. These conditions are specified by the intersection of the curve representing the surface energy balance equation (i.e., Eq. 1, wherein, for simplicity, only convective flux and reradiation losses are considered) and the convective heat flux curve (see Fig. 1, point A). Near extinction, the surface energy balance line (Eq. 1) moves higher (e.g., because of increased water application rate), and the steady state burning condition (point A) moves along the stable branch I of the gaseous convective curve until it reaches the maximum convective heat flux at the corresponding critical mass pyrolysis rate. Strictly speaking, critical extinction conditions exist when the surface energy balance equation curve is tangent to the convective heat flux curve (see Figure 1); this point nearly coincides with the maximum value of the convective heat flux (at $+A^*$, Figure 1), because: a) the slope of the

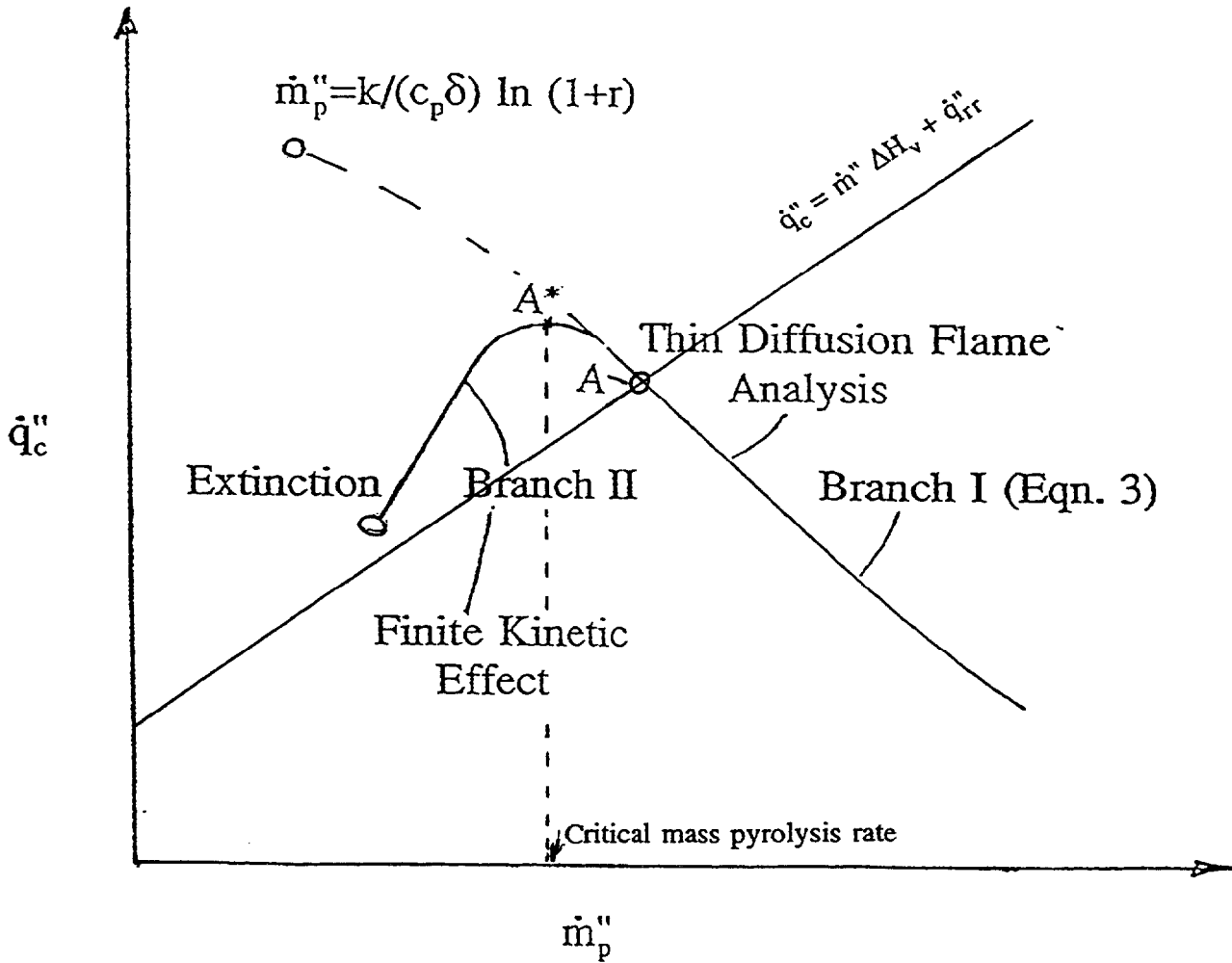


Figure 1. Expected convective heat flux variation with total mass pyrolysis rate and definition of steady pyrolysis state (point A) and critical conditions for extinction (point A*).

surface energy balance line (i.e., Eq. 4) is much smaller than the slope of the line to the left of A* in Figure 1; b), the convective heat flux curve near its maximum value is nearly flat.

2.1 Flame Convective Heat Fluxes

For simplicity, but with little loss of generality, we employ for illustration of the present approach the flow field associated with a stagnant film having thickness δ . In this situation, fuel is supplied on one side ($x = 0$) at a fixed rate \dot{m}_p'' , while at the other side ($x = \delta$) ambient oxygen concentrations prevail. A characteristic straining rate in this flow, which can affect the chemistry (Damkohler effect), is D/δ^2 , where D is the diffusivity which is assumed constant.

For Branch I, we have the following relations for the mass pyrolysis rate, \dot{m}_p'' , convective

$$\dot{m}_p'' = \frac{k}{c_p \delta} \ln(1+B) \quad (3)$$

mass transfer number, B , the convective heat flux \dot{q}_c'' , and flame sheet enthalpy, h_f :

$$B = \frac{Q_o Y_{o\infty} - (h_w - h_\infty)}{\Delta \bar{H}_v} = \frac{Q_o Y_{o\infty} - (h_w - h_\infty)}{\dot{q}_c''} \dot{m}_p'' \quad (4)$$

where the mass transfer number is defined as:

Eqs. (3) and (4) determine the gas combustion dynamics in Branch I (Fig. 1). Here k is the thermal conductivity, c_p is the specific heat of gas; Q_o is the heat released per mass of oxygen; $Y_{o\infty}$ is the ambient oxygen mass fraction; h_w , h_∞ are the gas enthalpy at the wall and ambient temperatures, respectively. At large blowing rates the convective heat flux drops exponentially to zero (because $\dot{q}_c'' \sim \dot{m}_p'' / \exp(\dot{m}_p'')$ from Eq. 3) and the flame sheet moves away from the pyrolyzing surface. At low blowing rates, as the flame sheet approaches the pyrolyzing surface, the convective heat flux increases and reaches a theoretical maximum value, see Eq. 7b, as proved subsequently.

The flame temperature (enthalpy) is given by:

$$h_f = h_w + \frac{Q_o Y_{o\infty} - (h_w - h_\infty)}{1 + r} - \frac{r}{1+r} \frac{\dot{q}_c''}{\dot{m}_p''} \quad (5)$$

where r is the fuel to air stoichiometric mass ratio:

$$r = \frac{Y_{o\infty} \nu_F M_F}{Y_{FT} \nu_o M_o} \quad (6)$$

The second term on RHS of Eq. 5 represents the adiabatic stoichiometric flame enthalpy and the last term in the RHS of Eq. 5 represents heat losses to the wall. In Eq. (6), ν_F , ν_o , are stoichiometric coefficients for fuel and oxygen, M_F , M_o are the molecular weights for fuel and oxygen, and Y_{FT} is the fuel concentration in the supply stream.

For infinitely fast kinetics, the maximum heat flux occurs when the flame sheet lies on the pyrolyzing surface and the flame temperature is equal to the wall temperature ($T_f = T_w$ or $h_f = h_w$); then Eq. 5 gives:

$$\frac{\dot{q}_c''}{\dot{m}_p''} = \frac{Q_o Y_{o\infty} - (h_w - h_\infty)}{r} \quad (7a)$$

where the mass pyrolysis rate is obtained from Eqs. (3) and (4) using $B = r$ from Eqs. 4 and 7a:

$$\dot{m}_p'' = \frac{k}{C_p \delta} \ln(1 + r) \quad (7b)$$

Eq. (7a) gives the maximum theoretical convective heat flux that can be applied to the surface (see broken line in Fig. 1); this situation occurs for infinitely fast kinetics in the gaseous phase. However, this situation cannot occur in practice because the surface temperature is much less than the flame temperature. Instead, the convective heat transfer will decrease at small values of pyrolysis rate following the Branch II as is shown in Fig. 1, because of partial flame quenching.

We continue now with the discussion of Branch II in Figure 1. Deviation from Branch I will occur as soon as chemical kinetics times become comparable to flow times; in this case, pyrolysis rates decrease and flames approach the pyrolyzing surface. To proceed further with our physical picture, we make use of key experimental results. We reproduce in Figure 2a results obtained by Corlett⁽⁹⁾ for heat transfer on horizontal porous burners supplying various gaseous fuels. Effects of fuel dilution by nitrogen are shown in Figure 2a, where solid symbols represent convective heat fluxes and open symbols represent total heat fluxes. We can observe that for high mass flux pyrolysis rates, convective heat fluxes are independent of dilution; this regime corresponds to Branch I of Figure 1.

There is another remarkable conclusion that can be drawn from inspection of Figure 2a; the mass pyrolysis flux at which the heat flux vs. mass flux correlation deviates from Branch I is inversely proportional to the degree of fuel dilution by nitrogen. At this point, the convective heat to the surface approaches a maximum value before it starts decaying until the flame reaches extinction. We will demonstrate that such a result is consistent with the proposition that the fuel concentration near the surface is constant (see Eq. 10d) when this deviation from Branch I occurs for the data included in Fig. 2a. This deviation is due, of course, to finite chemical kinetics. Nevertheless, we are using again the thin flame diffusion analysis to gain some insight into the physics of combustion near a pyrolyzing surface.

To demonstrate the validity of this statement, we have replotted the convective heat transfer data of fig. 2a in Fig. 2b by making the abscissa proportional to the fuel flow rate (supply flow times fuel concentration):

Fig. 2b shows that the net fuel flow rate at which heat flux is maximum is constant independent of the fuel dilution.

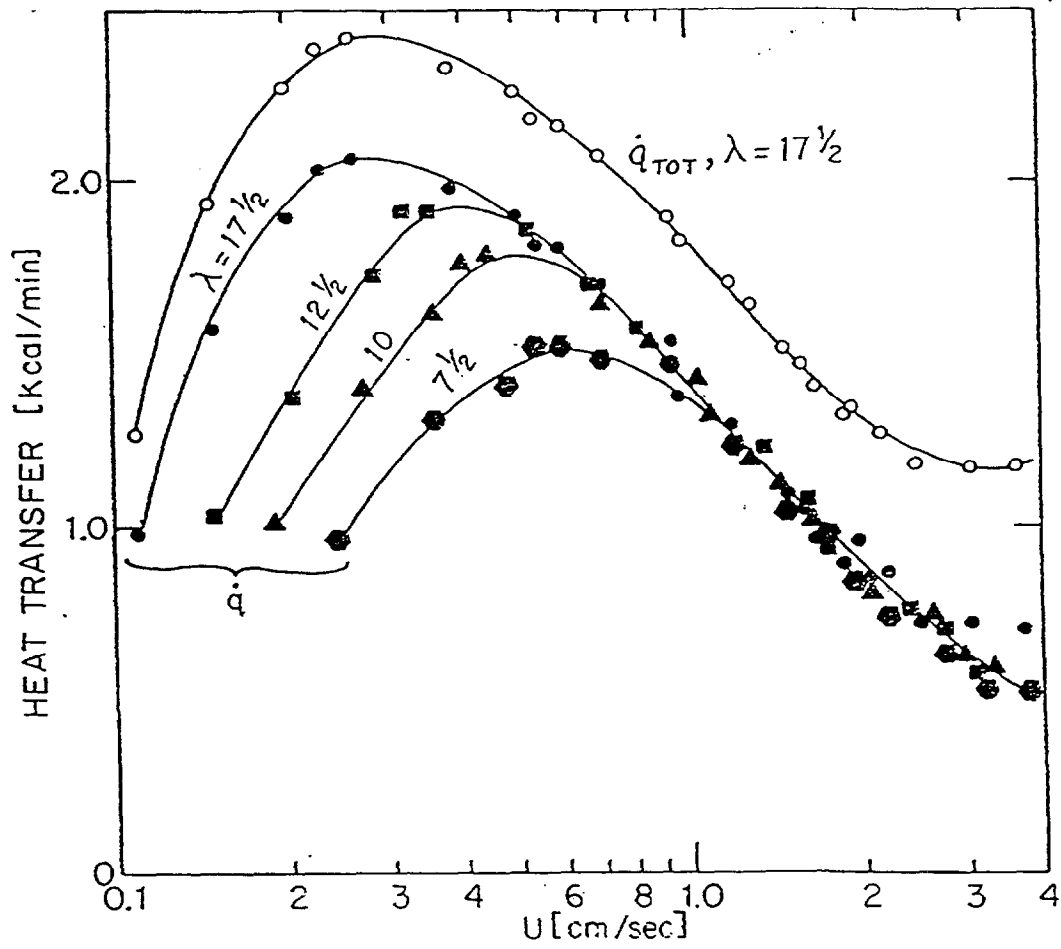


Figure 2a. Heat transfer data to the porous burner: Ethane-nitrogen system (porous burner diameter 4 in., lip height 1/4 in.). Solid symbols represent convective heat fluxes, open symbols total heat fluxes; λ is the air to fuel mole stoichiometric ratio, U is the average fuel gas velocity at the burner (from ref. 9).

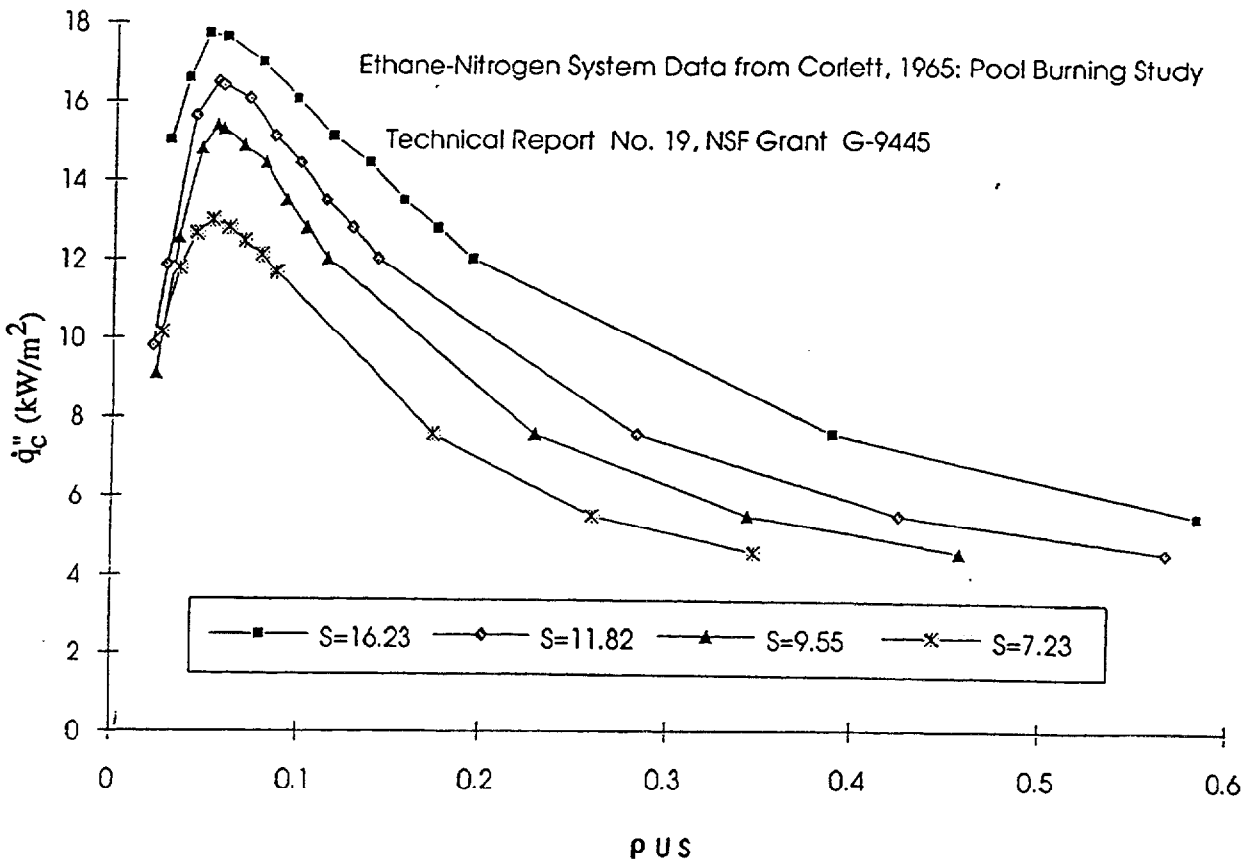


Figure 2b. Convective heat flux to the porous burner versus the mass flux multiplied by the air to fuel mass stoichiometric ratio (data are taken from Figure 2a). The abscissa is proportional to the ethane mass flux rate.

By using the present simplifying analysis (see Eqs. 3 to 7) and the experimental results Corlett⁽⁹⁾ (Figure 2b), we have deduced and proposed the following results:

The main conclusions are:

1. The critical pyrolysis rate (at which convective heat flux is maximum, Fig. 1) can be described by:

$$\left(\frac{\dot{m}_p'' c_p}{h_c} \right)_{crit} Y_{FT} = \text{constant depending on fuel gaseous kinetics} = C_e \quad (9)$$

but otherwise independent of flow field through the Damkohler number.

Here, we have used the fact that the convective heat flux coefficient h_c is equal to $\frac{k}{\delta}$ by definition, which is applicable for all the test conditions applicable in Fig. 2b.

2. By using Eqs. (3) and (4), we infer that at critical conditions

$$(Y_{FT} \ln(1+B))_{crit} = \text{constant} = C_e \quad \text{or}$$

$$Y_{FT} \ln \left(1 + \frac{\chi_A Y_{O_2} Q_o - (h_w - h_\infty)}{\dot{q}_c''} \dot{m}_p'' \right)_{crit} = \text{const} = C_e \quad (10a)$$

In Eq. (10a) we have modified the definition of convective mass transfer number (compare with Eq. 4) by introducing a combustion efficiency coefficient χ_A (to account for incompleteness of combustion) which will be determined experimentally. Condition (10a) can also be expressed in terms of fuel concentration at the surface by noting that the mass transfer number is also defined from:

$$Y_{FS} = Y_{FT} \frac{B - r\chi_A}{B + 1}$$

or

$$\frac{1}{1+B} = 1 - \frac{r\chi_A + \frac{Y_{FS}}{Y_{FT}}}{1+r\chi_A} \quad (10b)$$

where: Y_{FS} is the fuel concentration on the surface, and Y_{FT} is the fuel concentration in the supply stream. Thus, Eq. (10a) becomes

$$-Y_{FT} \ln \left(1 - \frac{r\chi_A + \frac{Y_{FS}}{Y_{FT}}}{1+r\chi_A} \right)_{crit} = C_e \quad (10c)$$

Because $r\chi_A$ is much less than one, Eq. (10c) can, near extinction, be approximated by:

$$Y_{FT} r\chi_A + Y_{FS} = \chi_A \frac{v_f M_F}{v_o M_o} Y_{\infty} + Y_{FS} = C_e \quad (10d)$$

Eqs. (10c) or (10d) provide a relationship between fuel and oxidant reactive species concentrations near extinction. It is interesting to emphasize that extinction criticality given by Eq. (9) is expressed in Eq. (10d) as a sum of fuel concentration at surface and ambient oxygen concentration which is a relation between chemical species being independent of heat transfer coefficient, h_c , or the fuel dilution, Y_{FT} .

We provide next a series of experimental results to validate Eqs. (10a) and (10c). These experimental results include:

- 1) surface heat flux measurements in a gaseous porous burner for fuels diluted by nitrogen⁽⁹⁾;
- 2) critical mass pyrolysis rates at reduced oxygen concentrations for various levels of external heat flux⁽¹⁰⁾ or material preheating⁽¹¹⁾;
- 3) critical mass pyrolysis rates at varying water drop application rates on the surface⁽¹²⁾.
- 4) critical mass pyrolysis rates of (transient) pyrolysis of a charring material exposed to various levels of external heat flux and/or oxygen concentrations, as performed as part of the present work.

2.2 Fuel Dilution by an Inert Gas

We have already presented these experimental results in Figs. (2a) and (2b). It is seen from Fig. (2b) that the mass flux of the fuel (not the total supplied mass flux) at critical conditions (i.e., maximum heat flux) is constant, independent of fuel dilution. The results in Fig. (2b) confirm the validity of our basic Eq. (9) because the heat transfer coefficient, h_c , is independent of fuel dilution in the present experiments, as explained next. The convective heat transfer coefficient (h_c in Eq. 9) is expected to be constant for different dilutions because it is only slightly dependent on temperature [$\Delta T^{1/3}$ (turbulent), $\Delta T^{1/4}$ (laminar)]⁷, and the flame temperature does not vary much with dilution of the fuel because the mass stoichiometric air to fuel ratio is large. This estimate is verified as is shown in Fig. 2a by: a) focusing on heat flux measurements (which are the same) at high mass flux ($U > \sim 1$ cm/s); and b) using Eqs. (3) and (4) for $\chi_A = 1.0$, which is applicable for flames away from critical conditions. Using these data in Figure 2a for $U = 2$ cm/s (where $\dot{m}_p'' = 24$ g/m²s, $\dot{q}_c'' = 6.9$ kW/m² as calculated from data in Fig. 2a) and Eqs. (3) and (4), we have estimated a value of $h_c = 10.0$ kW/m²K for the heat transfer coefficient in the present experiments ($Q_c = 13,100$ kJ/kg, $h_w = h_c$).

We have next used this heat transfer coefficient to determine the efficiency of combustion (χ_A in Eq. (10a)) at the critical mass flux rate as shown in Table I. An important conclusion from this table is that the combustion efficiency as defined by using Eq. (10a) is constant, i.e.,

TABLE I
COMBUSTION EFFICIENCY AT CRITICAL MASS FLUX
RATES FOR ETHANE-NITROGEN GAS BURNERS

Fuel Fraction Y_{FT}	Total Flow \dot{m}'' (g/m ² s)	\dot{q}_c'' (measured) (kW/m ²)	χ_A
1.	3.12	17.6	.68
.714	4.36	15.5	.65
.57	5.46	14.6	.65
.43	7.28	12.5	.63

independent of dilution at critical extinction conditions, wherein convective heat flux is maximum. We have also reproduced in Figure 2c another figure from Corlett's report⁽⁹⁾, which further supports the validity of Eq. 9. This figure shows the effect of "pool" diameter on the critical mass flux, namely, as the diameter, D, increases, the critical mass flux (i.e., mass flux at the maximum convective or total heat flux) decreases. By using Eq. (9), one can explain this behavior by observing that the convective heat transfer coefficient, h_c , increases as $D^{-1/4}$ for laminar conditions while it is independent of diameter for turbulent conditions. Laminar conditions exist for a diameter of $D = 2$ ", transition conditions for a diameter 4" and turbulent conditions for a diameter 7½" shown in Fig. 2c. The expected increase of critical mass flux as the diameter decreases from 4" to 2" would be by a factor $\left(\frac{4}{2}\right)^{1/4} = 1.19$ (assuming laminar flow conditions, for illustration), which

is consistent with the corresponding variation shown in Fig. 2c, as can be seen by inspection. This agreement is supported by further experiments presented in following sections, as well as by comparison with stagnation flow diffusion flame experiments on porous cylinders and their numerical solutions^(13,14,15), as discussed in the final section of this paper. We have presented evidence to support the argument that critical mass rates can be determined by using Eq. (9) or Eqs. (10a) and (10b). For the ethane-nitrogen mixture in Figures 2a, 2b, and 2c, we have found the following values.

$$\left(\frac{\dot{m}_p'' C_p Y_{FT}}{h_c} \right)_{crit} = C_e = .312 \quad (11a)$$

$$-Y_{FT} \ln \left(1 - \frac{r\chi_A + \frac{Y_{FS}}{Y_{FT}}}{1 + r\chi_A} \right)_{crit} = .312 \quad (11b)$$

$$Y_{FT} \ln \left(1 + \frac{\chi_A Y_{\infty} Q_o - (h_w - h_s)}{\dot{q}_c''} \dot{m}'' \right)_{crit} = .312 \quad (11c)$$

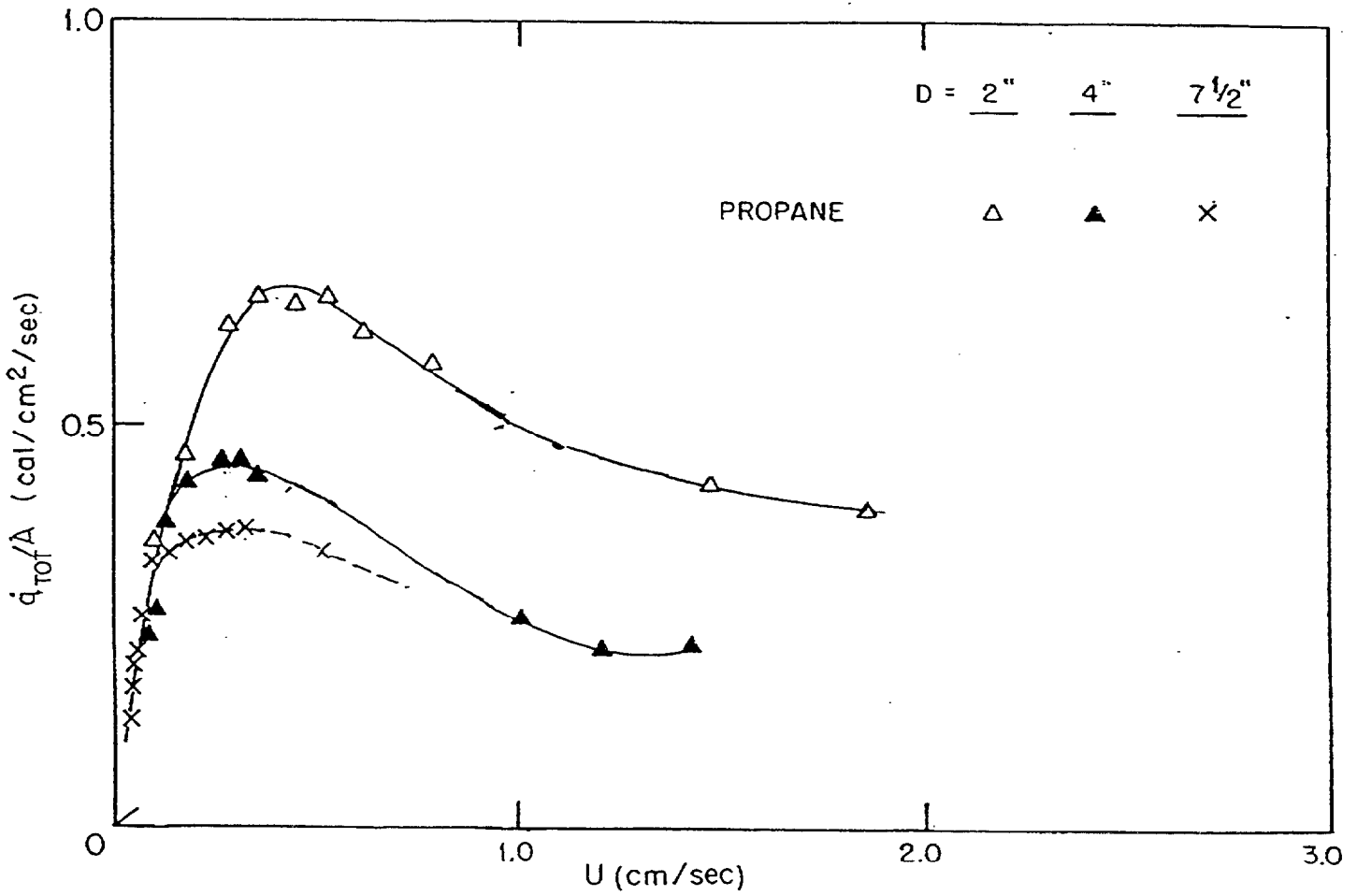


Figure 2c. Effects of diameter on critical fuel mass flux and total heat transfer flux to the burner for propane; U is the average fuel gas velocity at the burner (from ref. 9).

where $\chi_A = .65$ as shown in Table I. The constant in Eq. 11 will depend on the nature of the fuel and the diluent, which in the present experiment was an inert gas (N_2); its value could in general be determined experimentally.

2.3 Oxidant Stream Depletion by Nitrogen

In this section, we demonstrate how the results and modeling developed by using gaseous porous burner heat flux measurements can be applied for interpreting and analyzing critical mass pyrolysis rates for condensed fuels at extinction. We consider two sets of experiments, both for PMMA (polymethylmethacrylate) conducted at varying external heat fluxes⁽¹⁰⁾ and at various material initial preheating temperatures⁽¹¹⁾ of PMMA.

Results from the former case are shown in Figures 3a and 3b, and results from the latter case are shown in Figure 3c. Finally, in Figure 3d we plot all the data corresponding to extinction conditions for PMMA taken from Figures 3a, 3b and 3c. For each extinction condition, a point in Fig. 3d is defined having coordinates the mass pyrolysis at extinction (abscissa), and the total heat flux to the surface (ordinate). The total heat flux is calculated by applying an energy balance in the surfaces for cases plotted in Fig. 3a and Fig. 3c. For the data in Figure 3a corresponding to (molal) oxygen concentrations (.18, .19, and .21), critical conditions for extinction (namely, the level of external heat flux) have been determined by the intercept of the corresponding straight lines for pyrolysis rates with the straight horizontal line $\dot{m}'' = 5 \text{ g/m}^2\text{s} =$ mass pyrolysis rate at extinction.

We can make important observations by comparing data in Figure 3d with the analysis in the previous section:

a) For the same experimental setup^(10,11), the mass pyrolysis rates at extinction are independent of ambient oxygen dilution which is consistent with the finding that

$$\left(\frac{\dot{m}_p'' c_p Y_{FT}}{h_c} \right)_{crit} = C_e = constant \quad (12)$$

b) The pyrolysis rates at extinction, are, however, widely different for the two experiments $5 \text{ g/m}^2\text{s}^{(10)}$ compared to $19.2 \text{ g/m}^2\text{s}^{(11)}$ as shown in Figure 3d (from Fig.3c: $\dot{m}_p'' = \rho U = 1,200 \text{ kg/m}^3 \cdot .16 \cdot 10^{-4} \text{ m/s}$). This difference is explained by using Eq. (12), because the heat transfer co-

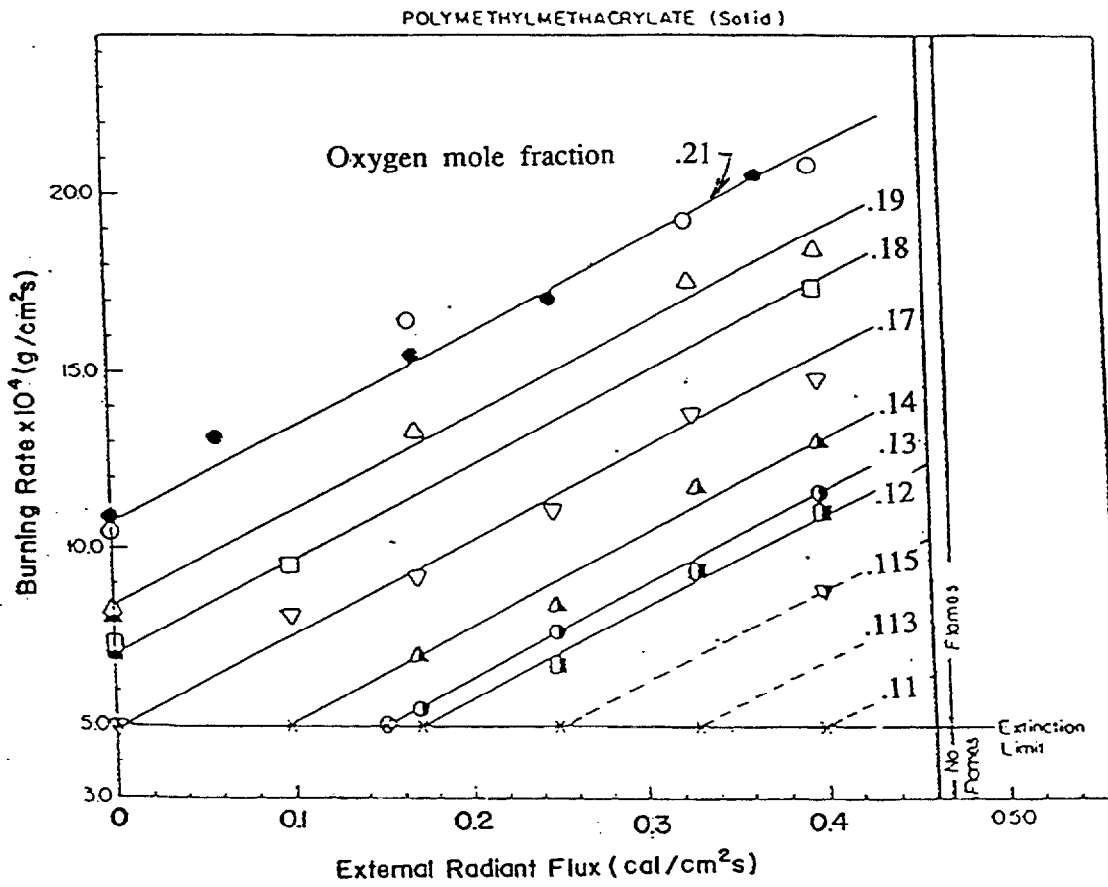


Figure 3a. Mass pyrolysis rate of PMMA as a function of external heat flux at constant values of various oxygen mole fractions, .21, .19, .18, .17, .14, .13, .12, .115 (from Tewarson¹⁰).

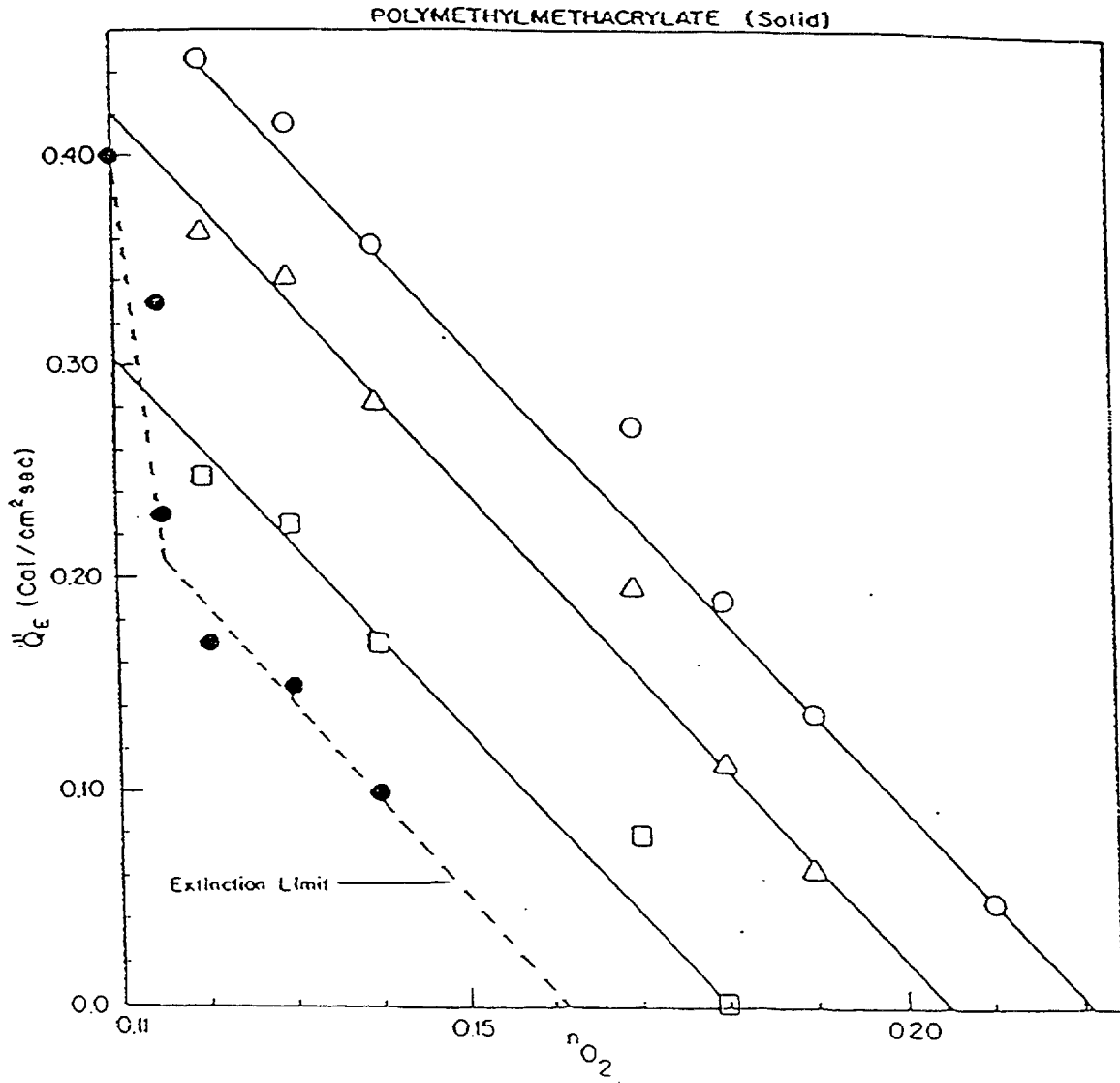


Figure 3b. Variations of external heat flux and mole fraction of oxygen for constant mass burning rates, $\dot{m}'' = 12, 10, 7, 5$ (extinction limit) g/m^2s . Same data as in Figure 3a (from Tewarson¹⁰).

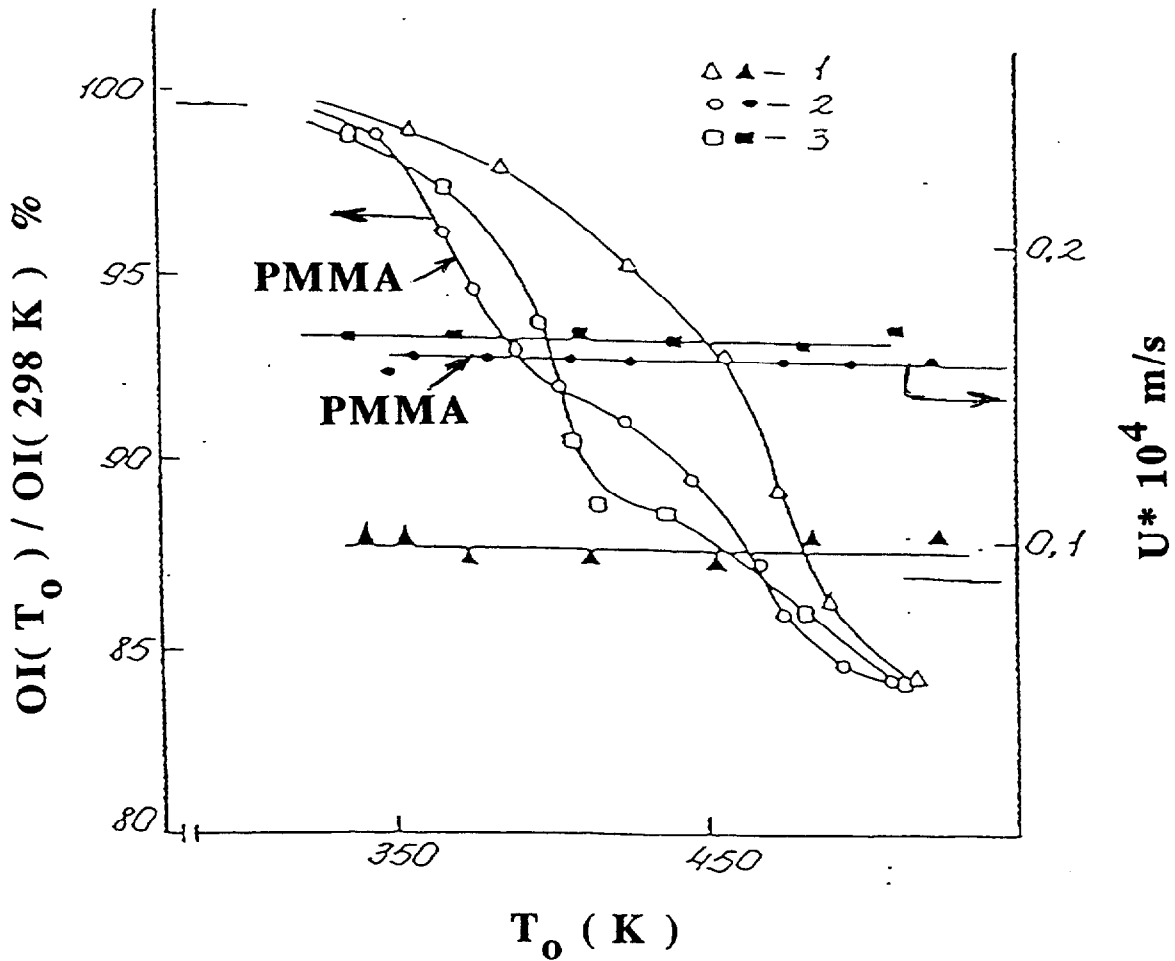


Figure 3c. The effect of initial sample temperature T_0 on normalized critical oxygen concentration $OI(T_0) / OI(298 K)$ and on linear regression rate U for a sample 1 cm in diameter : 1-PS; 2-PMMA; 3-POM (from ref. 11).

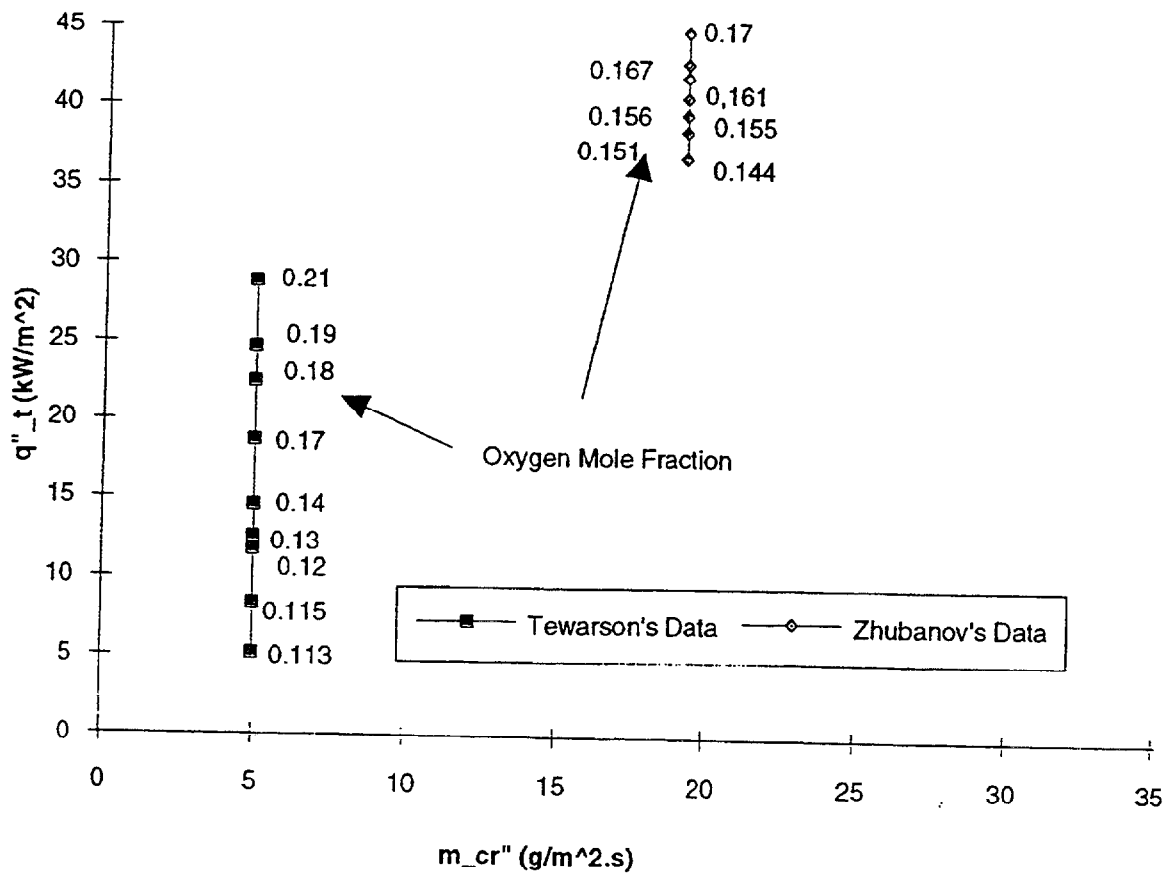


Figure 3d. Total heat flux at critical pyrolysis rate for PMMA results shown in Figures 3a and 3c.

efficient is widely different for these two experimental setups. The sample diameter for the data in Figure 3a is about 10 cm, whereas the sample diameter for the data in Figure 3c is 1 cm. Assuming that Eq. (12) is applicable, the ratio of heat transfer coefficients for the two tests should be $(19.2/5) = 3.84$, and the ratio of convective heat flux at critical conditions is also 3.84 as deduced by using Eq. 10a, namely, equal in both cases to the ratio of mass pyrolysis rates at extinction.

By using mass pyrolysis rate data for liquid pool fires⁽¹⁶⁾, we find that the ratio 3.84 of convective heat flux is indeed reasonable for a change of pool diameter from 10 cm (laminar to turbulent transition) (Fig. 3a) to 1 cm (laminar flow conditions) (Fig. 3c).

We can now compare the magnitude of flame heat fluxes to the surface as tabulated in Table II for the results reported in Figure 3a with magnitude of heat fluxes for the results reported in Figure 3c. Following our hypothesis that Eq. (12) is applicable for the same material in different experiments (i.e. different convective heat transfer coefficients) one can estimate the convective heat flux in Zhubanov and Gibov's experiment (Fig. 3c) by using Eqs. (2a) and (2b).

$$\frac{(\dot{q}_c'')_{3c}}{(\dot{q}_c'')_{3a}} = \frac{(\dot{m}'')_{3c}}{(\dot{m}'')_{3a}} = 3.84 \quad (13)$$

Thus, at ambient temperature (no preheating) of the sample the estimated heat flux at conditions of extinction (LO Index = 17% by volume) for the Zhubanov experiments⁽¹¹⁾ should be:

$$(\dot{q}_c'')_{3c} = (3.84) \dot{q}_{c\ 3a}'' = 55 \text{ kW/m}^2 \quad (14a)$$

where $\dot{q}_{c\ 3a}''$ is estimated from Table II at 14.3 kW/m^2 . This estimate in Eq. (14a) is close to the value estimated from energy balance Zhubanov's⁽¹¹⁾ experiments:

$$(\dot{q}_c'')_{3c} = \dot{m}'' \Delta H_v + \dot{q}_{rr}'' = 45 \text{ kW/m}^2 \text{ (see also Fig. 3d)} \quad (14b)$$

if one ignores other heat losses from the sample and various experimental uncertainties⁽³⁾. In making the comparison between results in Figs. 3a and 3c, we have assumed that the properties of PMMA in the two experiments are the same. The analysis in this section demonstrates that the hypothesis proposed based on gaseous burner experiments is consistent with extinction experiments in condensed materials.

TABLE II
HEAT FLUXES FOR PMMA (Fig. 3a)

Mole Fraction of Oxygen	Mass Fraction of Oxygen	Total Heat* Flux (kW/m ²)	Convective** Heat Flux (kW/m ²)
.21	.23	29.8	18.2
.19	.21	24.3	16.31
.18	.20	22.4	15.3
.17	.19	18.7	14.4
.14	.16	14.6	11.51
.13	.146	11.6	10.2
.115	.13	8.29	8.6***
.113	.127	5.15	8.34
.11	.124	2.02	8.06

$$\begin{aligned} \dot{q}_f'' &= \dot{m}'' \Delta H_v + \dot{q}_{rr}'' - \dot{q}_e'' \\ \Delta H_v &= 1848 \text{ k J/kg} \\ \dot{q}_{rr}'' &= \sigma T_p^4 = 9.5 \text{ kW/m}^2 \end{aligned}$$

**Use Eq. (9), (10) with assumed $\chi_A = .65$ (see Table I), and
 $Q_o = 13,100 \text{ kJ/kg}$, $\dot{m}'' = 5 \text{ g/m}^2\text{s}$, $h_c = 13.61 \text{ W/m}^2\text{K}$.

***The last three points represent extinction by quenching of the gaseous phase and not by interaction of flames with the pyrolyzing surface, compare with Fig. 3b.

III

CRITICAL PYROLYSIS RATES FOR VARYING SURFACE WATER DROP APPLICATION RATES

We apply the present theory and analysis for the explanation and prediction of critical pyrolysis rates when water drops are applied (by sprinklers or nozzles) on a surface for extinction. Experimental results are shown in Figure 4 from Magee and Reitz⁽¹²⁾ for burning of a vertical PMMA sample. Based on observations and considering the drop size⁽¹²⁾ and the surface temperature at pyrolysis, cooling of the surface occurs by dropwise (not film) evaporation. Near the material surface a flow of pyrolyzing gases is mixed with the steam produced by water evaporation. This situation is similar to the dilution of fuel by inert agents discussed in Section 3.1 (although steam may not be inert).

It is evident from Figure 4 that at extinction the mass flux of the condensed material is nearly constant at a value of 4 g/m²s at different water application rates, which correspond to different fuel dilutions. This observation is again consistent with our main result given by Eq. (9). The estimated heat transfer coefficient for vertical wall fires is $h_c \approx 10 \text{ W/m}^2\text{K}$. It is also straightforward to calculate the total heat flux to the surface by using an energy balance:

$$\dot{q}_t'' = \dot{m}'' \Delta H_v + \dot{m}_w'' \Delta H_w + \dot{q}_{rr}'' - \dot{q}_e'' \quad (15)$$

where \dot{m}'' is the fuel pyrolysis rate, ΔH_w is the energy for water drop vaporization, and \dot{q}_e'' is the imposed external heat flux.

It is remarkable that this calculation provides almost the same total flame heat flux:

$$\dot{q}_t'' = 19.5 \text{ kW/m}^2 \pm 1 \text{ kW/m}^2 \quad \text{at extinction independent of the water application rate.}$$

This result is not consistent with estimates of (convective) heat flux based on the present theory (compare also with table I), which predicts that the heat flux will drop, although not much, as the water application rate increases because of increased fuel dilution. Table III tabulates the estimated convective heat flux levels.

After considerable effort to understand the observed discrepancy, we have contributed the difference in the heat flux to the surface between theory (Table III - dilution effects) and measure-

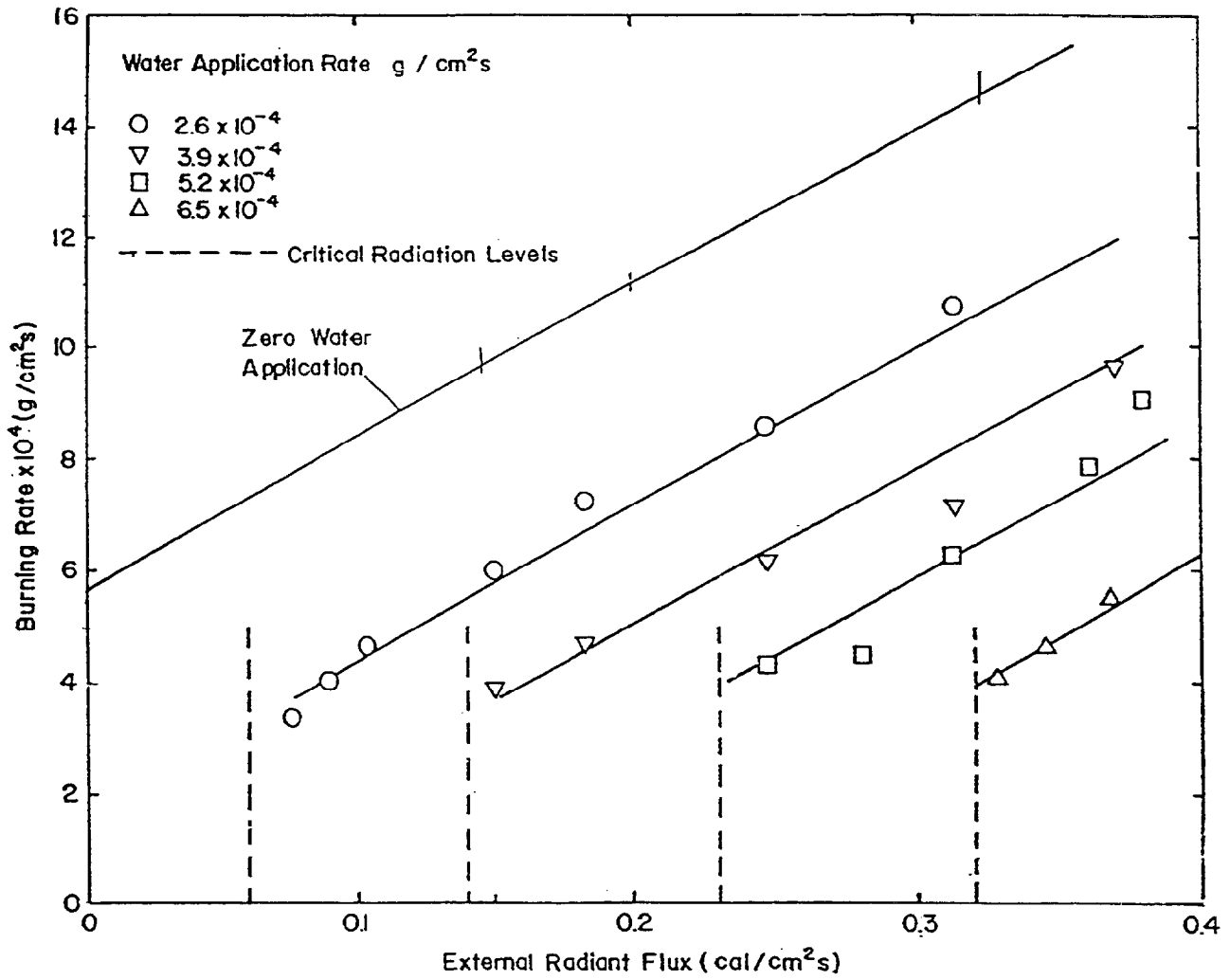


Figure 4. Burning rate of vertical PMMA slabs versus external radiant flux for various water application rates (ref. 12).

(total heat flux = 19.5 kW/m² fixed independent of water application rate) to two factors:

1) increase of radiation by water vapor produced by evaporation as water application rates increase;

2) increase of combustion efficiency (with increased water application rates) near extinction which was assumed (based on results in Section 2.1.1) to be $\chi_A = .65$ for the estimates of convective heat flux listed in Table III. Regardless of the appropriate reason and explanation, the experimental results suggest that the total flame heat flux at extinction is not affected by water application rates owing to compensating effects. Moreover, Figure 4 can be used to conclude that even for a fixed water application rate and increasing external heat flux (e.g., $\dot{m}_w'' = 2.6 \text{ g/m}^2 \text{ s}$) the total flame heat flux remains constant about equal to 19.5 kW/m².

There is another important comment regarding the effects of water application on the surface, especially the lack of any effect on the flame: although water vapor concentration is high at the surface (see Table III), the vapor concentration at the flame, where stoichiometric conditions prevail, is small, because it is reduced relative to the surface value proportionally to the stoichiometric ratio (thus for water application rate 2.6 g/m²s the vapor concentration near the flame is $.39/ (.61)(8.8) = 7.5\%$, and for water application rate 6.5 g/m²s, the vapor concentration

near the flame is $\frac{.62}{(.38)8.5} = 19\% \left(= \frac{(1 - Y_{FT})}{Y_{FT} (S + 1)} \right)$.

TABLE III
ESTIMATED CONVECTIVE HEAT FLUX AT EXTINCTION IN
WATER APPLICATION TESTS - DILUTION EFFECTS (SEE FIG. 4)

Water Application g/m ² s	Dilution of Fuel* Y _{FT}	Convective Heat Flux (calculated)** q _c " (kW/m ²)
2.6	.61	11.5
3.9	.51	10.7
5.2	.43	9.8
6.5	.38	9.1

*Assuming total instant evaporation.

**Use Eqs. (9) and (10) with $\chi_A = .65$, $Q_o = 13,100$ kJ/kg, $\dot{m}'' = 4$ g/m²s, $h_c = 10$ W/m²K. If $\chi_A = 1.0$ values of \dot{q}_c'' in Table III increase by a factor of 1/.65. Dilution of fuel (Y_{FT}) is calculated as the ratio of material mass flux to the sum of this value and the water mass flux.

IV

CRITICAL PYROLYSIS RATES AT EXTINCTION FOR CHARRING MATERIALS

To further validate the present approach and demonstrate a practical experiment for measuring critical mass pyrolysis rates, we have performed extinction experiments in a flammability apparatus available at FMRC, a diagram of which is shown in Fig. 5⁽¹⁷⁾. Particle board samples (diameter 9.65 cm, thickness, 1.9 cm) can be exposed to various levels of external heat flux and at various levels of oxygen concentration of ambient air. Mass loss histories, species concentrations, oxygen depletion and heat release rates are obtained using a load cell and gas analysis of the products of combustion collected by a hood⁽¹⁷⁾, as shown in Fig. 5. To speed up the initial ignition process, we have spread a few milliliters of acetone on top of the particle board for running the present experiments. Figs. 6a, 6b, 6c show measurements of mass loss (pyrolysis) rate, oxygen depletion and carbon monoxide in which a particle board sample was exposed to 35 kW/m² external heat flux at ambient conditions. Following the initial spike in mass loss rate (Fig. 6a) which corresponds to acetone consumption, particle board starts pyrolyzing and burning. Subsequently, the mass loss rate increases to a maximum value and then starts decreasing owing to char formation. During this period, flaming combustion occurs until the heat release rate and the pyrolysis rate decrease below a critical value. Flaming was observed to stop both visually and also by the increase in CO production, as illustrated in Fig. 6c. The value of mass pyrolysis rate at which flaming combustion stops is 5.5 g/m²s, as obtained from Fig. 6a. Pyrolysis of particle board continues because of the presence of external heat flux.

In addition to the test shown in Fig. 6, we have performed similar tests using particle board samples for the following additional conditions: a) external heat flux 35 kW/m², oxygen concentration 30%; b) external heat flux 25 kW/m², oxygen concentration 21%; c) external heat flux 25 kW/m², oxygen concentration 30%.

For all these tests, the critical mass pyrolysis rate at extinction (when no flaming combustion occurs) is 5.5 g/m²s with an accuracy $\pm 4\%$.

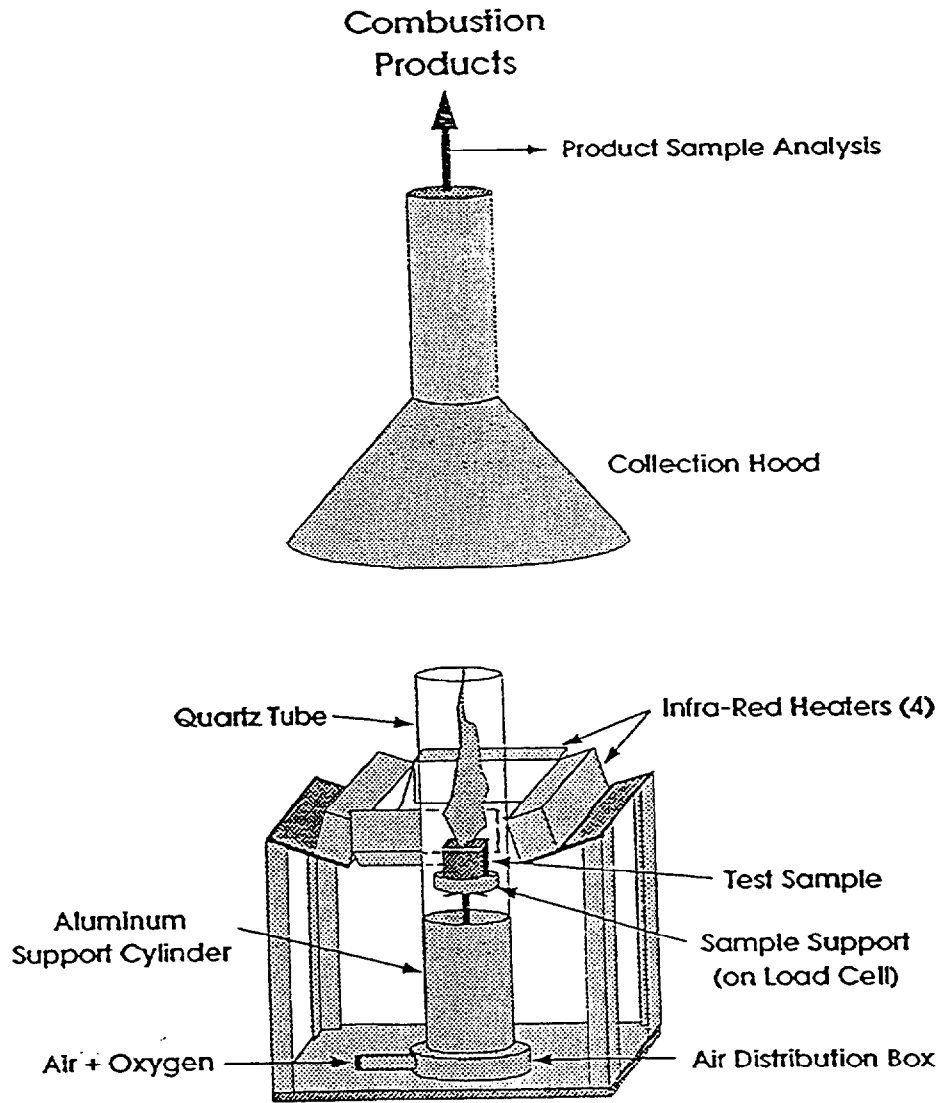


Figure 5. Factory Mutual Flammability Apparatus where both external heat flux and oxidant concentrations can be varied (ref. 17) for measuring extinction on solid fires.

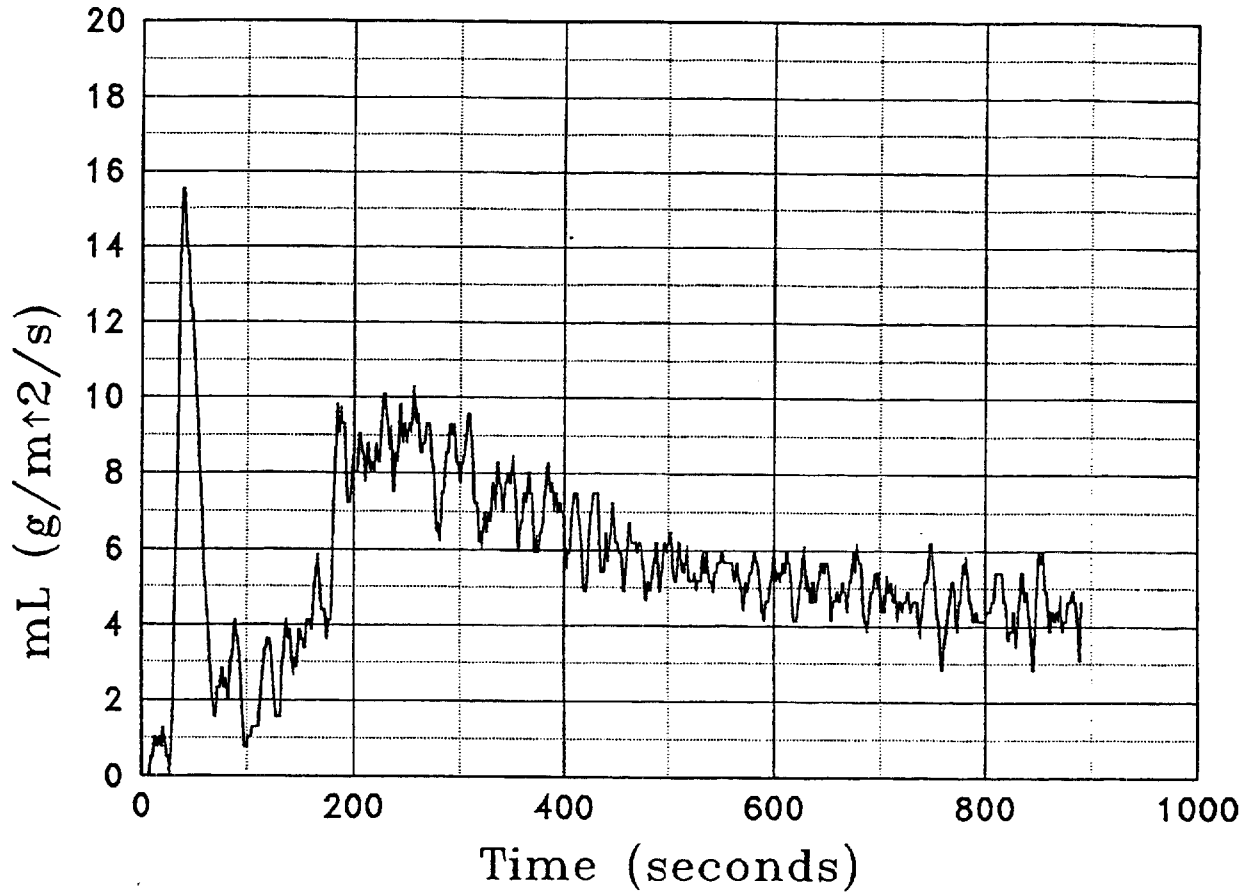


Figure 6a. Mass loss rate for particle board until flame extinction occurs at 400 s for the following conditions: external heat flux 35 kW/m^2 , at ambient air. Flame extinction is observed visually and supported by measurements as shown in Fig. 6b and 6c.

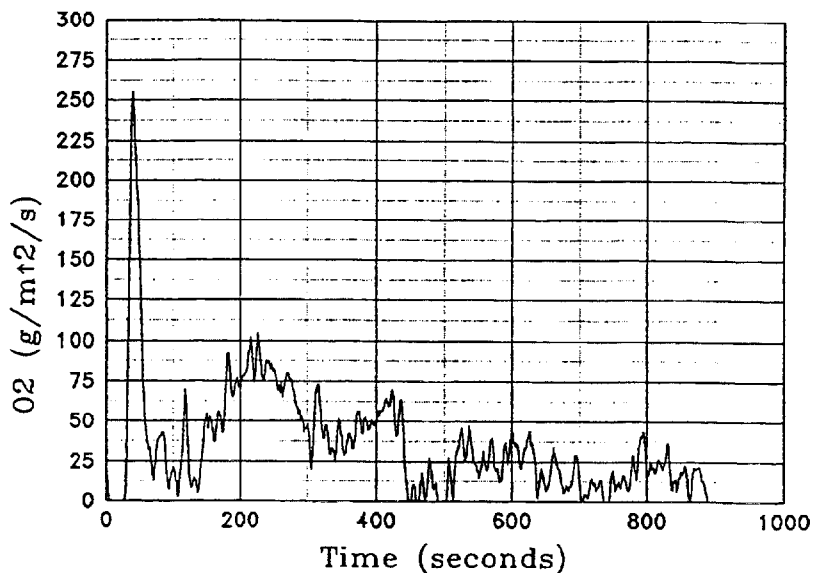


Figure 6b. Oxygen consumption for the test described in Fig. 6a: extinction is indicated to occur at 400 s.

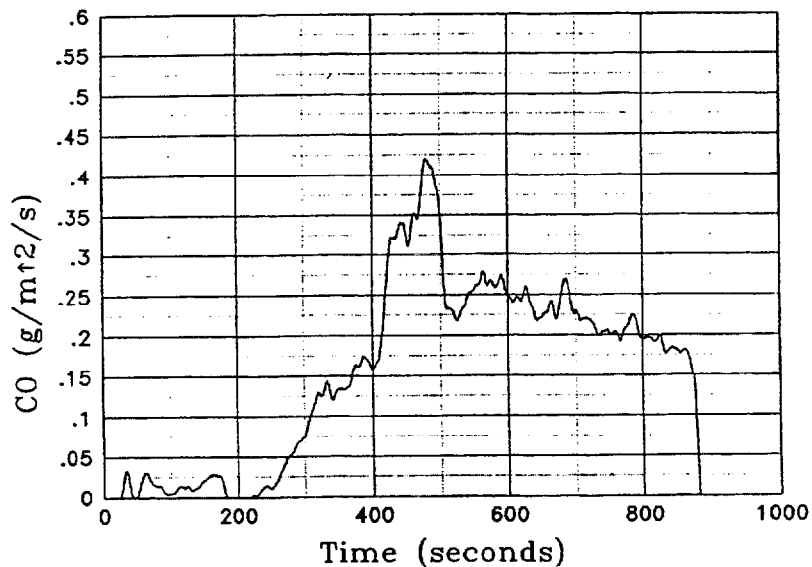


Figure 6c. Carbon monoxide production for test described in Fig. 6a: extinction is indicated to occur at about 400 s, where a sudden increase of CO production occurs.

V

DISCUSSION

We have proposed and validated a model that can characterize critical pyrolysis at extinction of flaming combustion when the mechanism involves interaction of the flames with the surface. The main results are included in Eqs. 9 and 10. We have also shown how these conditions for extinction can be measured in a flammability apparatus. The critical pyrolysis rate relation at extinction is applicable for various extinction agent applications including fuel dilution by inert agents, oxidant dilution by inert agents, or water application on the surface. The model does not only provide the critical mass pyrolysis rate, but also the convective heat flux to the surface (see Eqs. 10a, 10b and Tables I, II). We have also found that the mass transfer number should be modified by an efficiency coefficient (see Eq. 10c), which has been estimated to be constant for a given fuel ($\chi_A = .65$ for ethane gaseous burner, Table I), independent of dilution (or flow strain).

As we pointed out in the introduction, the present approach is physically explained and is more general than previous empirical approaches^(7,8).

It is also important to point out that the present results are consistent with Tsuji[13] experiments and numerical simulations (Tien⁽¹⁴⁾, Sibulkin⁽⁶⁾), although more work, including detailed chemistry (rather than global reaction rates) is needed to verify and delineate the limitations of the present model. We include a Figure 7 taken from Olsen and Tien's[14] paper to substantiate our claim here. This figure includes the extinction curve for a stagnation flow (experiments by Tsuji⁽¹³⁾), on a porous cylinder supplying a flammable gas. The ordinate is the dimensionless mass supply rate (essentially proportional to $\frac{\dot{m}_p'' C_p}{h_c}$ in our definition of critical condition). The abscissa is the

nominal strain rate. Extinction occurs when the mass supply rate becomes less than the value shown in Figure 7. Our extinction conditions correspond to the low straining rates in Figure 7, wherein extinction occurs by interaction of flame with the surface. In this regime, both experiments (notwithstanding buoyancy effects at very low straining rates) and numerical computations show that the dimensionless supply rate at extinction (which is

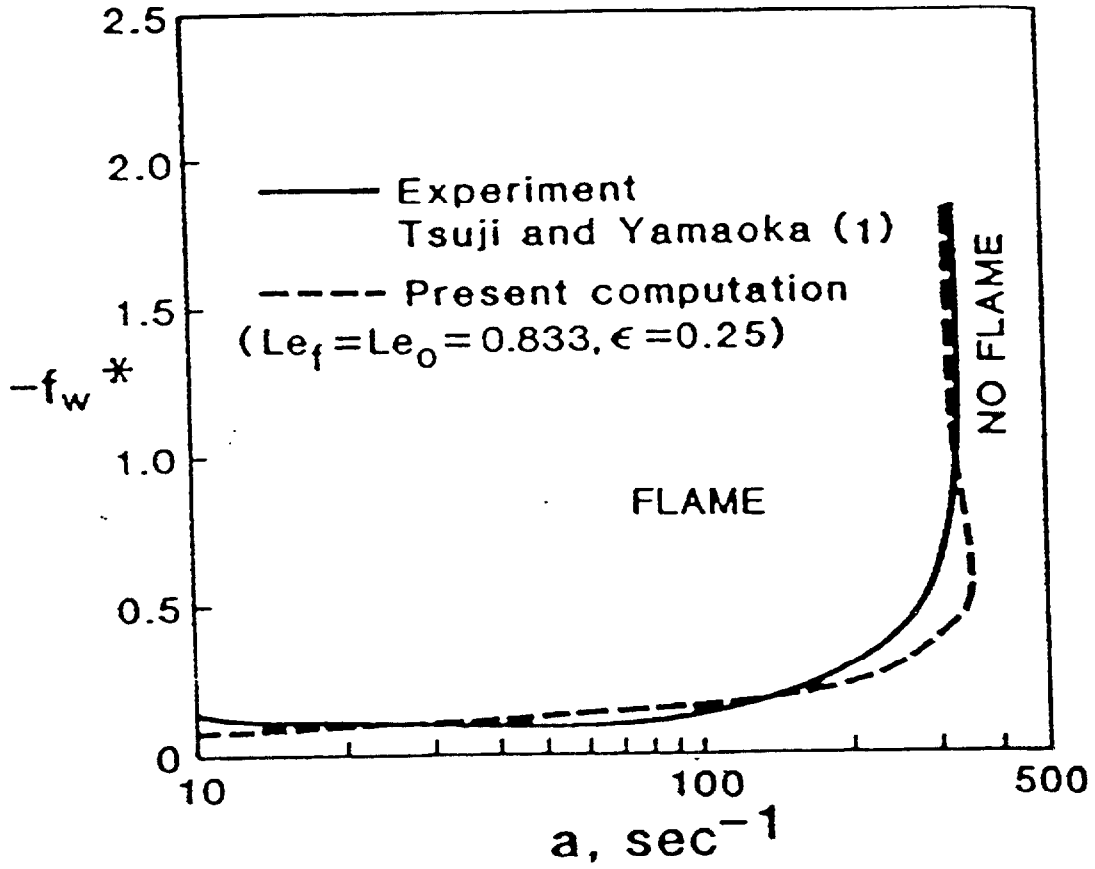


Figure 7. Computed and experimental mass flux at extinction conditions normalized by the heat transfer coefficient in terms of straining rate, α , in counterflow diffusion flame on a cylinder. At low straining rates, extinction mass flux is nearly constant (independent of straining rate) in accordance with present results (Eq. 9).

proportional to our parameter $\frac{\dot{m}_p'' C_p}{h_c}$ is constant and independent of straining rate, in consistency

with our model. It should be noted that extinction conditions in Figure 7 do not exactly correspond to extinction conditions in a condensed fuel (where maximum convective heat flux occurs).

For further validation of our model, additional work is needed and planned to numerically predict convective heat flux to the surface as mass pyrolysis rates decrease[18]. Detailed chemistry is recommended to help delineate the limitations of our model.

VI CONCLUSIONS

We have used experimental and numerical evidence to validate new extinction conditions for flames on solid materials when extinction occurs by interaction of flames with the surface. We have found, surprisingly, that these extinction conditions do not depend on the Damkohler number. These extinction conditions given by Eqs. (9), (10a) or (10d) allow determination both of the critical (extinction) mass pyrolysis rate (Eq. 9) and the heat flux at extinction (Eq. 10a). Expressed in the form of Eq. (10d), the extinction conditions provide a novel chemistry based formulation which shows that the sum of the fuel mass fraction near the solid surface and the ambient oxygen mass fraction corrected for stoichiometry and combustion efficiency is constant.

REFERENCES

1. Frank-Kamenetskii, D.A. "Calculation of Thermal Explosion Limits," Acta Phys.-chim, URSS 10, 365, 193.
2. Friedlander, S.K. and Keller, K.H., "The Structure of the Zone of Diffusion-Controlled Reaction," Chem. Engrg., Sci. 18, 365, 1939.
3. Fendell, P.E., "Ignition and Extinction in Combustion of Initially Unmixed Reactants," J. Fluid Mech., 21, 282-303 (1965).
4. Linan, A. and Williams, F.A., "Theory of Ignition of a Reactive Solid by Constant Energy Flux," Comb. Sci. Tech, 3, 91.
5. Law, C.K., "Asymptotic Theory of Ignition and Extinction in Droplet Burning," Combustion and Flame, 24: 89-98, 1975.
6. Sibulkin, M., "Free Convection Diffusion Flames from Burning Solid Fires," Prog. Energy Combust. Sci. 14: 195-212, 1988.
7. Beyler, C., "A Unified Model of Fire Suppression," J. of Fire Prot. Engr. 4 (1), pp. 5-16, 1992.
8. Rasbash, D.J., "Theory in the Evaluation of Fire Properties of Combustible Materials," Proceedings of the Fifth International Fire Protection Seminar, Karlsruhe, Germany, 1976, pp. 113-130.
9. Corlett, R.C. "Heat Transfer Data Summary - Pool Burning Study," Division of Eng. Applied Sciences, Eng. Science Laboratory, Harvard University, Technical Report 19, 1965.

10. Tewarson, A. and Pion, R.R., "Flammability of Plastics - I. Burning Intensity," *Combustion and Flame*, 26, 85-103, 1976.
11. Zhubanov, T.B. and Gibov, K.M., "Oxygen Index and Minimum Tasks of Polymer Combustion," *Fire and Materials*, 12, 169-172, 1988.
12. Magee, R.S., and Reitz, R.D., "Extinguishment of Radiation Augmented Fires by Water Sprays," *Fifteenth Symposium International on Combustion*, The Combustion Institute, Pittsburgh, PA, 1975.
13. Tsuji, H., "Counterflow Diffusion Flames," *Prog. Energy Combust. Sci.*, 8, 93-119, 1982.
14. Olson, S.L. and Tien, J.S., *Combust. and Flame*, 70, 161-170, 1987.
15. Oh, T.K., Lee, J.S., and Chung, S.H., *Int. J. Heat Mass Transfer*, 37, 2983-2900, 1994.
16. Mudan, K.J. and Croce, P.A., Chapt. 3-11 in *SFPE Handbook of Fire Protection Engineering*, 2nd Edition, NFPA, 1995.
17. Tewarson, A., "Generation of Heat and Fire Products," FMRC Report J.I. 0ROJ4.RC(3), 1995.
18. Vlachos, D.G., Schmidt, L.D., Aris, R., "Ignition and Extinction of Flames Near Surfaces: Combustion of CH₄ in Air," *AIChE, Journal*, 40: 1005-10017, 1994.

NIST-114 (REV. 11-94) ADMAN 4.09	U.S. DEPARTMENT OF COMMERCE NATIONAL INSTITUTE OF STANDARDS AND TECHNOLOGY	(ERB USE ONLY)	
<h1>MANUSCRIPT REVIEW AND APPROVAL</h1>		ERB CONTROL NUMBER	DIVISION
INSTRUCTIONS: ATTACH ORIGINAL OF THIS FORM TO ONE (1) COPY OF MANUSCRIPT AND SEND TO THE SECRETARY, APPROPRIATE EDITORIAL REVIEW BOARD.		PUBLICATION REPORT NUMBER NIST-GCR-98-746	CATEGORY CODE
		PUBLICATION DATE April 1998	NUMBER PRINTED PAGES
TITLE AND SUBTITLE (CITE IN FULL) Critical Mass Pyrolysis Rates for Extinction in Fires Over Solid Materials			
CONTRACT OR GRANT NUMBER GONANB4D1675	TYPE OF REPORT AND/OR PERIOD COVERED NIST-GCR-98-746		
AUTHOR(S) (LAST NAME, FIRST INITIAL, SECOND INITIAL) Delichatsios, Michael A.	PERFORMING ORGANIZATION (CHECK (X) ONE BLOCK) <input type="checkbox"/> NIST/GAITHERSBURG <input type="checkbox"/> NIST/BOULDER <input type="checkbox"/> JILA/BOULDER		
LABORATORY AND DIVISION NAMES (FIRST NIST AUTHOR ONLY)			
SPONSORING ORGANIZATION NAME AND COMPLETE ADDRESS (STREET, CITY, STATE, ZIP) Factory Mutual Research Corporation			
PROPOSED FOR NIST PUBLICATION <input type="checkbox"/> JOURNAL OF RESEARCH (NIST JRES) <input type="checkbox"/> MONOGRAPH (NIST MN) <input type="checkbox"/> LETTER CIRCULAR <input type="checkbox"/> J. PHYS. & CHEM. REF. DATA (JPCRD) <input type="checkbox"/> NATL. STD. REF. DATA SERIES (NIST NSRDS) <input type="checkbox"/> BUILDING SCIENCE SERIES <input type="checkbox"/> HANDBOOK (NIST HB) <input type="checkbox"/> FEDERAL INF. PROCESS. STDS. (NIST FIPS) <input type="checkbox"/> PRODUCT STANDARDS <input type="checkbox"/> SPECIAL PUBLICATION (NIST SP) <input type="checkbox"/> LIST OF PUBLICATIONS (NIST LP) <input type="checkbox"/> OTHER _____ <input type="checkbox"/> TECHNICAL NOTE (NIST TN) <input type="checkbox"/> NIST INTERAGENCY/INTERNAL REPORT (NISTIR)			
PROPOSED FOR NON-NIST PUBLICATION (CITE FULLY) <input type="checkbox"/> U.S. <input type="checkbox"/> FOREIGN		PUBLISHING MEDIUM <input type="checkbox"/> PAPER <input type="checkbox"/> CD-ROM <input type="checkbox"/> DISKETTE (SPECIFY) _____ <input type="checkbox"/> OTHER (SPECIFY) _____	
SUPPLEMENTARY NOTES			
ABSTRACT (A 2000-CHARACTER OR LESS FACTUAL SUMMARY OF MOST SIGNIFICANT INFORMATION. IF DOCUMENT INCLUDES A SIGNIFICANT BIBLIOGRAPHY OR LITERATURE SURVEY, CITE IT HERE. SPELL OUT ACRONYMS ON FIRST REFERENCE.) (CONTINUE ON SEPARATE PAGE, IF NECESSARY.) A novel chemistry based formulation for extinction is provided which shows that the sum of fuel mass fraction near the surface and the ambient oxygen mass fraction is constant. The extinction conditions are derived from simple analysis of combustion and heat transfer, and they are shown to be applicable for various experimental conditions such as fuel dilution by inert gas, oxygen dilution by inert gas, effects of external heat flux, material preheating, transient (charring) pyrolysis, including geometric effects which influence the critical mass pyrolysis rate through an effective heat transfer coefficient. Additional validation of the proposed extinction conditions is provided by numerical simulation reported in literature in the regime of low straining rates for a stagnation flow on a cylinder.			
KEY WORDS (MAXIMUM OF 9; 28 CHARACTERS AND SPACES EACH; SEPARATE WITH SEMICOLONS; ALPHABETIC ORDER; CAPITALIZE ONLY PROPER NAMES) Extinction; fire suppression; pyrolysis			
AVAILABILITY <input checked="" type="checkbox"/> UNLIMITED <input type="checkbox"/> FOR OFFICIAL DISTRIBUTION - DO NOT RELEASE TO NTIS <input type="checkbox"/> ORDER FROM SUPERINTENDENT OF DOCUMENTS, U.S. GPO, WASHINGTON, DC 20402 <input checked="" type="checkbox"/> ORDER FROM NTIS, SPRINGFIELD, VA 22161		NOTE TO AUTHOR(S): IF YOU DO NOT WISH THIS MANUSCRIPT ANNOUNCED BEFORE PUBLICATION, PLEASE CHECK HERE. <input type="checkbox"/>	